
SCALABLE INFERENCE FOR BAYESIAN MULTINOMIAL LOGISTIC-NORMAL DYNAMIC LINEAR MODELS

A PREPRINT

Manan Saxena
Pennsylvania State University, USA
manansaxena@psu.edu

Tinghua Chen
Pennsylvania State University, USA
tuc579@psu.edu

Justin D. Silverman
Pennsylvania State University, USA
JustinSilverman@psu.edu

October 10, 2024

ABSTRACT

Many scientific fields collect longitudinal count compositional data. Each observation is a multivariate count vector, where the total counts are arbitrary, and the information lies in the relative frequency of the counts. Multiple authors have proposed Bayesian Multinomial Logistic-Normal Dynamic Linear Models (MLN-DLMs) as a flexible approach to modeling these data. However, adoption of these methods has been limited by computational challenges. This article develops an efficient and accurate approach to posterior state estimation, called *Fenrir*. Our approach relies on a novel algorithm for MAP estimation and an accurate approximation to a key posterior marginal of the model. As there are no equivalent methods against which we can compare, we also develop an optimized Stan implementation of MLN-DLMs. Our experiments suggest that *Fenrir* can be three orders of magnitude more efficient than Stan and can even be incorporated into larger sampling schemes for joint inference of model hyperparameters. Our methods are made available to the community as a user-friendly software library written in C++ with an R interface.

Keywords Bayesian Time Series · Multivariate Analysis · Microbiome Data

1 INTRODUCTION

Many scientific fields collect longitudinal multivariate count data where the total number of counts is arbitrary (e.g., multinomial observations). These data are often called count compositional as the information in the data relates to the relative frequencies of the categories (Silverman et al., 2018). These data occur frequently in molecular biology (Espinoza et al., 2020), microbiome studies (Silverman et al., 2018; Joseph et al., 2020; Äijö et al., 2018), natural language processing (Linderman et al., 2015), biomedicine (Fokianos and Kedem, 2003), and social sciences (Cargnoni et al., 1997). Although the counting process used to collect these data is often modeled as multinomial, other sources of noise in the system being studied often lead to extra-multinomial variation. While some account for this extra-multinomial variability with multinomial-Dirichlet models (Mosimann, 1962), multinomial logistic-normal models are often superior, as they can account for both positive and negative covariation between multinomial categories (Aitchison and Shen, 1980; Cargnoni et al., 1997; Joseph et al., 2020; Silverman et al., 2018). Moreover, under suitable transformation (i.e., link function), the logistic-normal is multivariate Gaussian. This facilitates development of latent Gaussian models (Aitchison, 1982). Multinomial logistic-normal dynamic linear models are particularly appealing for count compositional time series due to their flexibility and expressiveness (Silverman et al., 2018; Joseph et al., 2020; Cargnoni et al., 1997).

Dynamic Linear Models (DLM) are a flexible approach to Bayesian time series analysis (West and Harrison, 2006). These are linear Gaussian state space models that can perform a wide range of time series decomposition tasks, forecasting, and smoothing. The models can express additive combinations of a wide range of auto-regressive, moving average, dynamic regression, seasonal, and polynomial trend processes (Prado et al., 2021, Chapter 4). Multinomial Logistic-Normal DLM (MLN-DLMs) have been successfully applied in multiple fields, including the social sciences (Cargnoni et al., 1997) and, more recently, the study of host-associated microbial communities (microbiomes) (Joseph et al.,

2020; Silverman et al., 2018). However, computational problems have limited wide-spread adoption of MLN-DLMs. These problems are highlighted by microbiome data which are often high dimensional (tens to hundreds of multinomial categories). In this regime, the lack of conjugacy between the multinomial and the logistic-normal makes many MLN-DLM models intractable. Silverman et al. (2022) recently proposed a theory suggesting that a wide range of Bayesian multinomial logistic-normal models, including MLN-DLMs, MLN Linear Models, and MLN Gaussian Process Regression models, can be efficiently and accurately inferred using a novel sampler with marginal Laplace approximation, the Collapse-Uncollapse (CU) sampler. While their method performs well for the later two classes, we found it fails on MLN-DLMs due to extreme numerical instability when applied to long time series.

This article develops efficient and accurate posterior inference for a broad family of MLN-DLMs. Our approach is inspired by the Collapse-Uncollapse sampler but uses a novel gradient filtering algorithm for *Maximum A Posteriori* (MAP) estimation and a novel algorithm for posterior uncertainty quantification, which we call the *Debiased Multinomial Dirichlet Bootstrap*. For brevity, we refer to this approach as *Fenrir*. As there are no general-purpose implementations of MLN-DLMs against which we can compare, we also develop an optimized Stan (Carpenter et al., 2017) implementation of our MLN-DLM model class. We provide optimized and user-friendly software implementations of both methods. Through real and simulated data studies, we find that Fenrir provides accurate posterior estimation while typically being three orders of magnitude more efficient than Stan. Finally, we discuss hyperparameter estimation within MLN-DLMs. We demonstrate that Gibbs sampling can be a practical solution for the task and discuss future directions.

This article is organized as follows: Section 2 provides an overview of related work. Section 3 presents our proposed approach, highlighting our key contributions. Section 4 demonstrates our approach through simulated and real microbiome data applications. Finally, we conclude with a discussion in Section 5.

2 RELATED WORK

While this work focuses on MLN-DLMs; for completeness, we review the broader inference of Bayesian MLN models. We summarise current approaches into four categories: Hamiltonian Monte Carlo (HMC) and Markov Chain Monte Carlo (MCMC) methods, data augmentation techniques, variational inference methods, and collapse-uncollapse methods.

Hamiltonian Monte Carlo (HMC) and MCMC Methods: Early studies of MLN-DLMs used Metropolis-within-Gibbs samplers (Cargnoni et al., 1997). These methods could only scale to a few multinomial categories (Silverman et al., 2022). More recently, MLN (and MLN-DLMs) have been inferred using HMC (Grantham et al., 2020; Äijö et al., 2018; Silverman et al., 2018) with Stan implementations being particularly popular (Äijö et al., 2018; Silverman et al., 2018). Still, these methods either required strong low-rank assumptions (Grantham et al., 2020); could only be applied to a subset of observations at a time (Äijö et al., 2018); or could only scale to 10 multinomial categories and could only handle simple random-walk dynamics (Silverman et al., 2018). Even with these restrictions many methods still took hours to infer (Silverman et al., 2018).

Data Augmentation Techniques: Pólya-Gamma data augmentation, which introduce Pólya-Gamma random variables within a Gibbs sampling scheme, has become a popular approach to inferring a wide variety of Bayesian logistic models (Polson et al., 2013). These methods have even been applied in certain multinomial logistic-normal tasks (Glynn et al., 2019). However, these methods have a critical limitation: In multinomial logistic-normal models, Pólya-Gamma random variables cannot be block-updated while maintaining the logistic-normal model form (Linderman et al., 2015). As a result, the number Gibbs steps required to collect a single posterior sample from these models grows linearly with the number of multinomial categories. In practice, this makes the approach infeasible for the tasks considered in this article.

Variational Inference: More recently, variational inference has been proposed for MLN models (Joseph et al., 2020; Silverman et al., 2022). In fact, Joseph et al. (2020) developed a scalable variational approximation to MLN state-space models. However, their method lacks the full generality of the MLN-DLMs class we consider here, i.e., their method only models random-walk dynamics within the state space. Additionally, Silverman et al. (2022) also studied variational inference for MLN linear and Gaussian process regression models, concluding that variational inference was more computationally expensive and produced less accurate posterior estimates than Collapse-Uncollapse (CU) methods.

Collapse-Uncollapse Methods: More recently, Silverman et al. (2022) studied a wide class of Bayesian MLN models that are *Marginally Latent Matrix-t Processes* (MLTPs). MLTPs are defined by a shared marginal form. These include generalized linear and Gaussian process regression models as well as generalized DLMs (e.g., MLN-DLMs). Their approach leveraged the shared marginal form through a novel *Collapse-Uncollapse* (CU) sampler (see Section 3.1 for

details). While they showed that the CU sampler alone improved inferential efficiency, they also derived a closed-form Laplace approximation to the Collapse step for MLN models, which yielded the most significant gains. While Silverman et al. (2022) suggest their approach could be used for MLN-DLMs, we found their proposed approach is numerically unstable in practice (see Supplementary Section 6).

3 PROPOSED METHOD

We consider a $D \times T$ matrix of multivariate count measurements Y with elements Y_{dt} representing the number of observed counts in category $d \in \{1, \dots, D\}$ at time point $t \in \{1, \dots, T\}$. While later sections consider studies that contain multiple time series or time series with missing observations, for simplicity, this section assumes only a single time series with equally spaced observations.

This article considers the same class of MLN-DLMs introduced in Silverman et al. (2022):

$$\begin{aligned} Y_{.t} &\sim \text{Multinomial}(\pi_{.t}) \\ \pi_{.t} &= \phi^{-1}(\eta_{.t}) \\ \eta_t^T &= F_t^T \Theta_t + v_t^T \quad v_t \sim \mathcal{N}(0, \gamma_t \Sigma) \\ \Theta_t &= G_t \Theta_{t-1} + \Omega_t, \quad \Omega_t \sim \mathcal{N}(0, W_t, \Sigma) \\ \Theta_0 &\sim \mathcal{N}(M_0, C_0, \Sigma) \\ \Sigma &\sim IW(\Xi, \nu) \end{aligned}$$

where ϕ refers to any log-ratio transformation from the D -simplex to $(D - 1)$ -real space and $N(M, A, B)$ denotes a matrix normal distribution. For computational efficiency we choose $\phi = ALR_D$ where $ALR_D(x) = (\log \frac{x_1}{x_D}, \dots, \log \frac{x_{D-1}}{x_D})$. However, this choice does not limit the generality of our method as posterior samples can be easily transformed into a wide variety of other log-ratio coordinates systems (Pawlowsky-Glahn et al., 2015, Appendix A.3). The latent log-ratio coordinates, η_t , are modeled with a multivariate DLM (Prado et al., 2021, Chapter 10). These are a flexible family of time series models which, through specification of the terms F_t, G_t, W_t, γ_t , can model a wide variety of polynomial trend, seasonal, and dynamic regression processes, as well as additive combinations of such processes. A thorough review of the capabilities of this model class is provided by (Prado et al., 2021, Chapters 4 and 10). Here, we simply note the each of the $D - 1$ dimensions of η_t is modeled with Q state space dimensions, such that the state space Θ_t is a $Q \times (D - 1)$ matrix. This implies that F_t is a Q -vector representing how the state-space is related to the log-ratios of the latent multinomial probabilities η_t ; G_t is a $Q \times Q$ matrix describing the deterministic component of the states temporal evolution; W_t is a $Q \times Q$ covariance matrix representing covariation between the stochastic component of the states temporal evolution; Σ is a $(D - 1) \times (D - 1)$ covariance matrix representing covariance between each of the $D - 1$ dimensions of the model; and γ_t is a positive-valued scalar (typically set to 1) which allows analysts to model interventions (Prado et al., 2021, Chapter 4). Hyperparameters Ξ, ν, M_0 and C_0 define the model priors.

3.1 Overview of Model Inference

Our goal is produce samples from the posterior $p(\Theta, \Sigma, \eta \mid Y)$ where $\Theta = (\Theta_1, \dots, \Theta_T)$ and $\eta = (\eta_1, \dots, \eta_T)$. We are particularly interested in the posterior marginal $p(\Theta \mid Y)$, as Θ is often of more scientific interest than η or Σ . Our approach is inspired by the CU sampler (Silverman et al., 2022). We first produce samples from the *collapsed model's* posterior $p(\eta \mid Y)$. Then, we *uncollapse* each sample by sampling from the posterior conditional $p(\Theta, \Sigma \mid \eta)$. In what follows, we focus on the collapse step (sampling from $p(\eta \mid Y)$), as an efficient and exact algorithm for the uncollapse step already exists (see the smoothing recursion provided Supplementary Section 7).

For scalability, we follow Silverman et al. (2022) and seek approximate solutions to the collapsed sampling problem. We develop our solution in two steps: First, we develop an efficient approach for MAP estimation within the collapsed model $p(\eta \mid Y)$. Then, we use that MAP estimate to produce samples from an approximate posterior $q(\eta \mid Y) \approx p(\eta \mid Y)$.

3.2 Efficient MAP Estimation of η

We obtain MAP estimates of η within the collapsed model:

$$\hat{\eta} = \underset{\eta \in \mathbb{R}^{(D-1) \times T}}{\text{argmin}} [-\log p(\eta \mid Y)]$$

By Bayes rule, the collapsed model can be partitioned into two parts:

$$-\log p(\eta | Y) \propto - \underbrace{\sum_t \log \text{Multinomial}(Y_{\cdot t} | \phi^{-1}(\eta_{\cdot t}))}_I - \underbrace{\log p(\eta)}_{II}$$

By developing efficient algorithms for calculating each of these terms and their gradients, we can obtain the MAP estimate via first-order optimization methods.

Term I is straight forward to calculate and the gradients were already provided by Silverman et al. (2022). Those results are reproduced in Supplementary Section 8.

To calculate Term II, we use the fact that

$$\log p(\eta) = \sum_t \log p(\eta_t | H_{t-1}^T)$$

where $H_{t-1} = (\eta_{t-1}, \dots, \eta_1)$. Following results in Silverman et al. (2022), each $p(\eta_t | H_{t-1}^T)$ follows a multivariate T distribution:

$$p(\eta_t | H_{t-1}^T) \sim t_{\nu_{t-1}}(f_t, q_t \Xi_{t-1})$$

where ν_{t-1} , Ξ_{t-1} , f_t , and q_t are given by the multivariate DLM filtering recursion provided in Supplementary Section 7. Gradients of $\log p(\eta)$ are therefore the sum of the gradients of each term $p(\eta_t | H_{t-1}^T)$. In Supplementary Section 8, we derive computationally efficient representations of those gradients.

3.3 The Debiased Multinomial Dirichlet Bootstrap

Before introducing our approach, we provide some context. At least within the microbiome field, researchers have reported success by approximating each observation $Y_{\cdot t}$ with independent Bayesian Multinomial Dirichlet models (Friedman and Alm, 2012; Fernandes et al., 2014; Nixon et al., 2023, 2024):

$$\begin{aligned} Y_{\cdot t} &\sim \text{Multinomial}(\pi_{\cdot t}) \\ \pi_{\cdot t} &\sim \text{Dirichlet}(\alpha) \end{aligned}$$

where α is a D -vector with $\alpha_d > 0$. The posterior is given by $\pi_{\cdot t} \sim \text{Dirichlet}(Y_{\cdot t} + \alpha)$. Those authors use each posterior sample $\pi^{(s)} = (\pi_{\cdot 1}^{(s)}, \dots, \pi_{\cdot T}^{(s)})$ in subsequent calculations, ultimately summarizing those calculations over S posterior samples. We call this the Multinomial Dirichlet Bootstrap.

Inspired by that approach, we approximate $\prod_t q(\eta_t) \approx p(\eta | Y)$ where each $q(\eta_t)$ is defined by

$$\begin{aligned} \pi_{\cdot t} &\sim \text{Dirichlet}\left(\phi^{-1}(\hat{\eta}_{\cdot t}) \cdot \sum_d Y_{dt} + \alpha\right) \\ \eta_{\cdot t} &= \phi(\pi_{\cdot t}) \end{aligned}$$

We call this as the *Debiased Multinomial Dirichlet Bootstrap*. The intuition behind this approximation is as follows. In the context of our MLN-DLM model, we expect the posterior mean of the Multinomial bootstrap would be biased compared to the true posterior due to the assumed independence between each observation $Y_{\cdot t}$. In contrast, our MAP estimate $\hat{\eta}$ does not make this independence assumption. Moreover, arguments in Silverman et al. (2022) suggest the MAP estimate is a good estimate for the posterior mean $\mathbb{E}[\eta | Y]$ for MLN-DLMs. As a result, we construct our approximating posterior around this MAP estimate. Our procedure is equivalent to the log-ratio transformation of the Multinomial bootstrap but using pseudo-observations, $\tilde{Y}_{\cdot t} = c\phi^{-1}(\hat{\eta}_{\cdot t})$, to ensure the maximum likelihood corresponds to our MAP estimate. We choose the proportionality constant $c = \sum_d Y_{dt}$ to maintain the strength of evidence of the original data. We call this approximation, the *Debiased Multinomial Dirichlet Bootstrap* and use it to approximate the collapsed step of the CU sampler.

3.4 Computational Complexity

Our approach also addresses scalability issues in prior methods. Note that, even without the issues of numerical instability, Silverman et al. (2022) proposed solution requires a Laplace approximation which leads to an overall computational complexity $\mathcal{O}((N \times [D - 1])^3)$. Despite this, their method is still more efficient than alternative methods. Our approach is far more efficient. Computational complexity in our approach is dominated by the uncollapse step which requires ST inversions of one $Q \times Q$ and one $[D - 1] \times [D - 1]$ symmetric positive-definite matrix. Hence, the computational complexity of our approach is of the order $\mathcal{O}(ST(Q^3 + [D - 1]^3))$.

3.5 Handling Missing Observations

Our approach can easily be extended to handle missing-at-random observations through modifications of the filtering recursion given in Supplementary Section 7. In this recursions, at each time-point t , the posterior for Θ_{t-1} is projected forwards in time to serve as the prior for Θ_t ; the data is then used to update the prior to a posterior for Θ_t . When a missing observation is encountered, the posterior for Θ_t is equal to the prior – no updating is performed. This simple modification is provided in Supplementary Section 9.

3.6 Multiple Time Series

Our approach can be naturally extended to $K > 1$ time series, with each series potentially having different length T_k . We allow each time series to have its own state parameters Θ_t , while sharing information about other parameters (e.g., Σ) between the series. Operationally, we concatenate these time series and treat them as a single time series with $T = \sum_{k=1}^K T_k$ time points, then smooth each time series in isolation. The only exception is that our updates for Ξ and ν during filtering and smoothing share information between the series. Full algorithmic details, along with a graphic depiction of our procedure, are provided in Supplementary Section 10.

3.7 Hyperparameter Inference

The preceding subsections described an efficient approach to state and covariance estimation $p(\Theta, \Sigma | Y)$ for any MLN-DLM model. MLN-DLM models are specified by the quadruple G_t, F_t, W_t, γ_t . The model class is expanded when hyperparameters within this quadruple are learned from the data. While much of this topic is beyond the scope of the present article, we demonstrate a simple, yet effective approach to a joint Bayesian inference of the state variance W_t . In later sections, we discuss potentially more complicated, yet likely more efficient approaches to hyperparameter inference. As a demonstration, we assume the state variance is time-invariant and diagonal $W_t = W = \text{diag}(w_1, \dots, w_Q)$ and extend the MLN-DLM model class by including a prior:

$$w_q \sim \text{InvGamma}(a_q, b_q)$$

We can generate samples from the posterior $p(\Theta, \Sigma, \eta, w_1, \dots, w_Q | Y)$ using Gibbs updates detailed in Supplementary Section 11.

3.8 Software Implementation

We provide software implementations of our inference method for MLN-DLMs, called *Fenrir*. This is implemented as an R package, with the majority of computations implemented as a C++ header library using the Eigen and Boost libraries for efficient linear algebra and random number generation. We use an L-BFGS optimizer (provided by the RcppNumerical library; Qiu et al. (2023)) for MAP optimization.

Beyond *Fenrir*, we also developed an optimized Stan (Carpenter et al., 2017) implementation of our MLN-DLM models so that we had something against which to compare. Like *Fenrir*, our Stan implementation is optimized using the CU sampler which improves efficiency and stability of the method Silverman et al. (2022). Like *Fenrir*, Stan also implements an L-BFGS optimizer which is nearly identical to the RcppNumerical implementation.

The code for the *Fenrir* package is available at (github.com/manansaxena/fenrir), and the code for the optimized Stan implementation, along with all code required to reproduce the results in the following sections, is available at (github.com/manansaxena/fenrir_paper_code).

4 EXPERIMENTATION AND RESULTS

We compare *Fenrir* and our Stan implementation (henceforth simply called Stan), in terms of efficiency and accuracy of MAP estimation and uncertainty quantification. In all aspects, we consider Stan the gold-standard in terms of accuracy. All experiments were performed independently on identical hardware, each allocated with 256GB RAM, 16 cores, and restricted to a 48-hour upper limit on wall run-time. Due to Stan’s limitations, we restricted our experiments to moderate- and low-dimensional datasets to respect the run-time restriction.

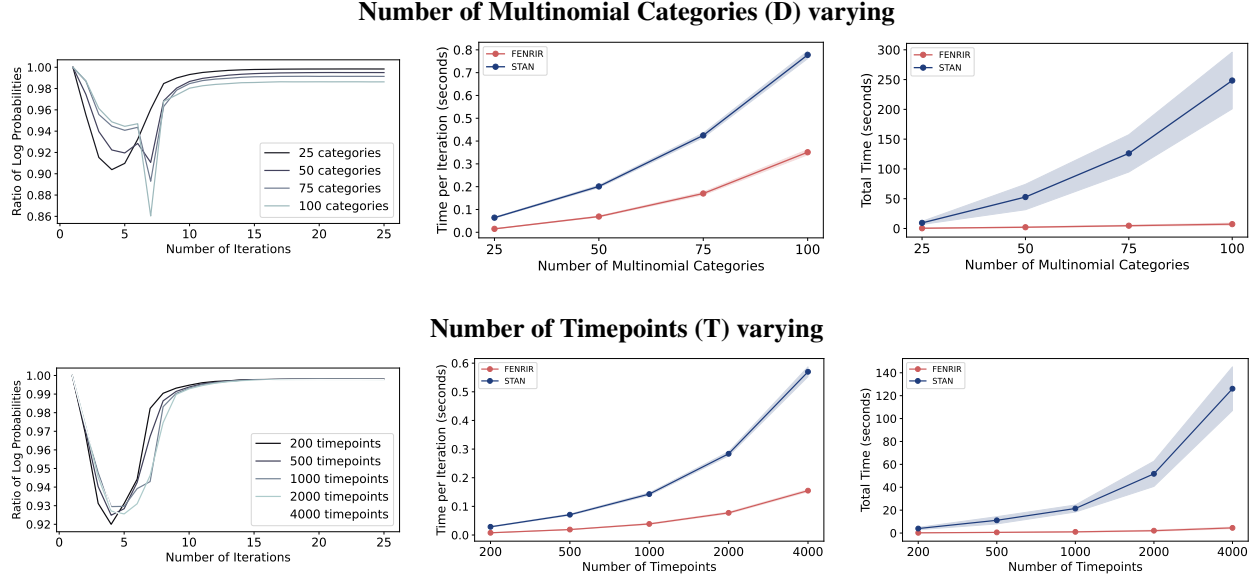


Figure 1: **Comparison of optimization results for MAP estimation of η applied to simulated data.** We compared Fenrir to our Stan implementation of MLN-DLMs at various Numbers of multinomial categories D (with T fixed at 600) and time points T (with D fixed at 30). Results represent mean and standard deviations calculated over 10 simulations at each combination of D and T . Fenrir converges to the same optima as Stan but in fewer iterations (first column), less time per iteration (second column), and substantially lower overall runtime (third column).

4.1 Simulations

To ensure our simulations do not diverge, we simulate a mean reverting random walk:

$$\begin{aligned}\Theta_t &= \Theta_{t-1} + \Omega_t, & \Omega_t &\sim \mathcal{N}(0, 0.45, \Sigma) \\ \Sigma &\sim IW(I, D + 3)\end{aligned}$$

We simulated multiple time series sharing the parameter Σ between them and introducing randomly missing observations. Full simulation details are provided in Supplementary Section 12. Fenrir and Stan were fit to identical data using identical priors.

4.1.1 Maximum A Posteriori (MAP) Estimation

We simulated data by varying the number of time points T and multinomial dimension D . Each simulation was repeated 10 times for each combination of T and D to account for random variation in the simulation. The results are summarized in Figure 1.

Let $l_s(ite)$ and $l_f(ite)$ denote the log-probabilities of the Stan and Fenrir models at a particular iteration, respectively. We compute the ratio $r = l_s(ite)/l_f(ite)$ in the first column of Figure 1. As the number of iterations increase, $r \rightarrow 1$ indicating Fenrir and Stan reach the same optimal. Still, at all iterations, $r < 1$ indicating Fenrir reached the optima in fewer steps. Fenrir also took less time per iteration (second column of Figure 1). Overall this led to substantial decreases in wall run-time (third column of Figure 1). These effects become more dramatic in higher dimensions. For large D or T , MAP optimization in Fenrir was often 20-30 times faster than Stan while obtaining identical estimates.

We attribute these results to Fenrir’s use of closed-form gradients, which likely result in less numerical error compared to Stan’s automatic differentiation approach, which involves significantly more computations. Note it is unlikely these effects are due to differences in L-BFGS implementations. Review of both code bases suggest only slight differences in stopping criteria between the implementations. Such differences could not explain the first and second columns of Figure 1.

4.1.2 Uncertainty Quantification

For interpretability, we compare the accuracy of uncertainty quantitation in Fenrir and Stan by visualization. For brevity, we show results for a small simulation ($D = 3, T = 300$) in the main text and leave results from a larger

($D = 10, T = 300$) simulation to Supplementary Section 12 as our conclusions were identical in both cases. Further experimental details are also provided in Supplementary Section 12.

We compare the computational efficiency of each method using the Number of Effective Samples per Second (NEff/s), a metric recommended by the Stan authors, as it accounts for autocorrelation between samples (Carpenter et al., 2017).

Figure 2 shows the mean and 95% credible intervals of the inferred states Θ from both Fenrir and Stan. There is almost perfect agreement between the posterior’s 95% intervals and the posterior means estimated by both methods. Yet Fenrir produces nearly 800 times more effective samples per second of η than Stan, with Fenrir achieving 12,329 NEff/s compared to Stan’s 15.39 NEff/s. To translate this into wall time: in this simulation, Fenrir generates 2000 effective samples (i.e., independent samples) in 0.16 seconds, while Stan requires 129.95 seconds to produce the same number. In short, at least for these simulations, Fenrir has virtually no approximation error while being substantially more efficient.

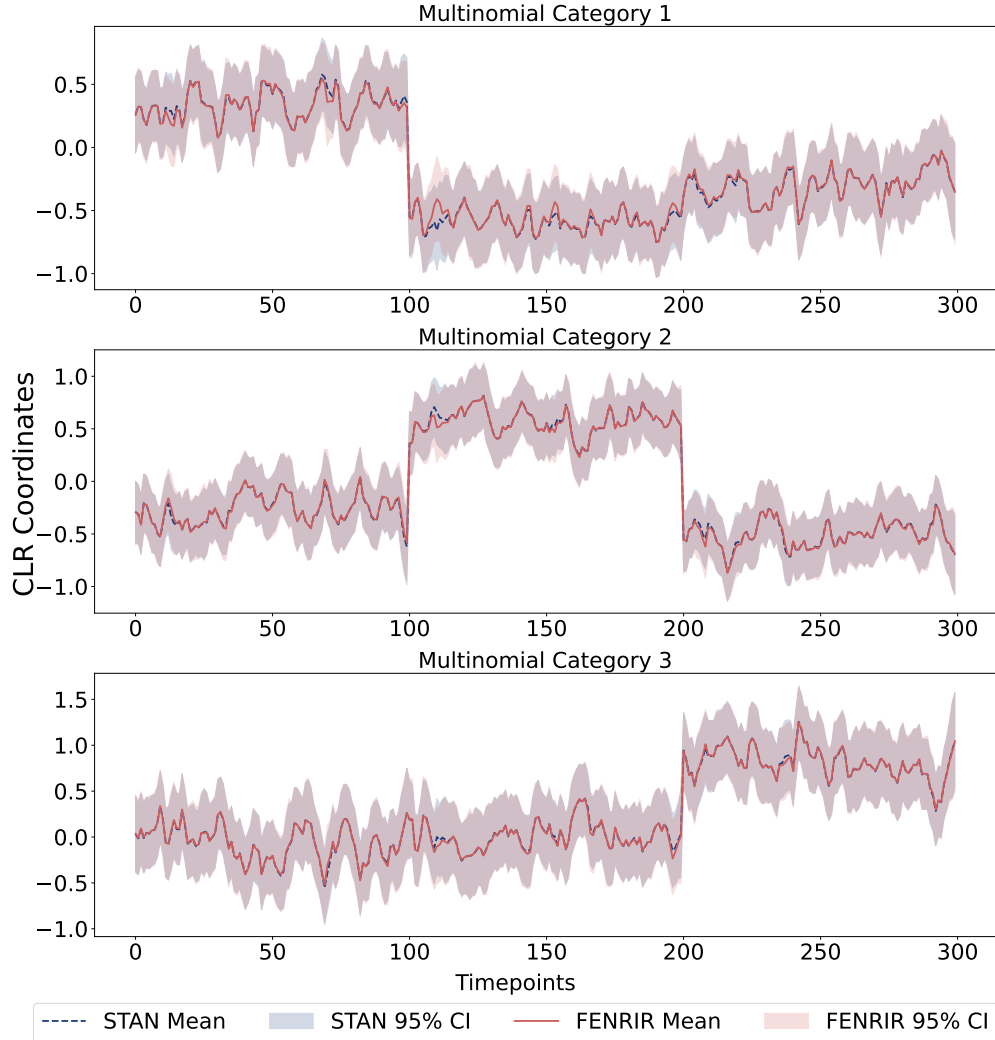


Figure 2: **Posterior mean and credible intervals for Θ from Fenrir and our Stan implementation.** The posterior is depicted using centered log-ratio (CLR) coordinates, with each coordinate corresponding to a different multinomial category. *To preempt potential confusion:* both the means and 95% credible intervals of Stan and Fenrir are plotted but hard to distinguish as there is almost perfect agreement between the estimates.

4.2 Real Data

We compared Fenrir and Stan on a previously published, finely-sampled, artificial gut microbiome time series. This dataset consists of 4 concurrent time series each consisting of daily measurements over 1 month with high-resolution hourly samples collected during a 5 day period around day 23 (Silverman et al., 2018). This study was previously used

to motivate and validate MLN-DLM models (Silverman et al., 2018). As mentioned in Section 2, those prior methods took hours to days to obtain accurate posterior estimates and were limited to modeling random walks within the state space for computational tractability. Here we show that we can reproduce those results in a fraction of the time using Fenrir. Moreover, in Supplementary Section 14 we show that Fenrir can model more complicated state-space dynamics.

We also use this analysis to demonstrate hyperparameter inference. In both Stan and Fenrir, we infer the state variance $W_t = W = \text{diag}(w_1)$ by adding a $w_1 \sim \text{InvGamma}(a_1, b_1)$ prior to the MLN-DLM model, as discussed in Section 3.7. In this respect, we expect our simple Gibbs sampler to underperform compared to Stan. Gibbs sampling is often less efficient than methods like HMC or MCMC, where the sampler can move in multiple directions at each iteration (e.g., updating both W and Θ). In contrast, our Gibbs sampler alternates between updates to W and updates to Θ . Still, we find that state estimation using Fenrir is so much more efficient than Stan that it compensates for these limitations, remaining substantially more efficient than our optimized Stan model. In later sections, we discuss how more complicated methods like slice-sampling Murray and Adams (2010), could provide further improvements. As in our simulation experiments, both Fenrir and Stan fit identical models: identical data, likelihoods, and priors (see Supplementary Section 13 for details).

As in our simulation studies, MAP estimation was substantially more efficient in Fenrir than Stan. At a given value of W , Fenrir produces the same estimate as Stan but in a fraction of the time (see Supplementary Section 13). Overall, Stan took 13.96 seconds for MAP estimation, while Fenrir took only 0.85 seconds.

The posterior estimates of W were nearly identical, with Fenrir estimating a posterior mean and 95% credible interval of 0.146 (0.132–0.164), and Stan estimating a posterior mean and 95% credible interval of 0.143 (0.128–0.159). In terms of Θ the Fenrir-based Gibbs sampler also produced nearly identical posterior estimates to Stan. For brevity, Figure 3 shows 4 dimensions of the estimated posterior for Vessel 2 from both methods (an extended plot showing all dimensions and all vessels is provided in Supplementary Section 13). We purposefully highlight the two dimensions where our Gibbs sampler does the worst (Synergistaceae and Fusobacteriaceae) and two that have received particular attention in previously published analyses (Rikenellaceae and Enterobacteriaceae).

Our Fenrir-based Gibbs sampler was least accurate at the very start of the time series for the taxa Synergistaceae and Fusobacteriaceae (Figure 3). We attribute this is due to the abundance of zero counts at the beginning of the time series, when total microbial load in the vessels was low immediately after inoculation (Silverman et al., 2018). Synergistaceae and Fusobacteriaceae are two of the lowest abundance taxa, which introduces substantial uncertainty regarding their true relative abundance in the presence of so many zero counts. Yet, even in this worst-case scenario, the dynamics inferred by our Fenrir-based Gibbs sampler and Stan are largely in agreement: both method agree that these two taxa were at extremely low relative abundance, and there is substantial overlap between their posterior 95% credible intervals. Outside of these 3-4 time points, in these two taxa, there is near-complete agreement between the two methods’ posterior means and credible intervals.

Our Fenrir-based Gibbs sampler produces nearly identical results to Stan for key taxa. As in prior analyses Silverman et al. (2022, 2018), the Fenrir-based Gibbs sampler infers a dramatic decrease in the relative abundance of Rikenellaceae following the starvation of Vessels 1 and 2, which occurred between experimental days 11-13. Consistent with prior analyses, we also observe the eventual recovery of the community as Rikenellaceae’s relative abundance returns to prior baseline levels. Beyond these large-scale dynamics, our model also captures known fine-scale oscillatory behavior in the Enterobacteriaceae. Similar to previous analyses, we find that this taxon exhibits sub-daily oscillations – observable when hourly samples were taken during a 5 day period around day 23.

Overall, the approximate posterior estimated by the Fenrir-based Gibbs sampler was nearly identical to that estimated by Stan. However, as expected, posterior samples of W from the naive Gibbs sampler were more correlated than Stan’s (Supplementary Section 13). Despite this, the accelerations provided by Fenrir were enough to overcome this limitation. Overall, the Fenrir-based Gibbs sampler produced effective samples at a rate of approximately 2.5 times Stan (Fenrir: 0.74 NEff/s; Stan 0.31 NEff/s). In the next section, we discuss alternatives to Gibbs sampling that could improve these results.

5 DISCUSSION

We have developed efficient and accurate posterior inference for Multinomial Logistic-Normal Dynamic Linear Models (MLN-DLMs). This family of models is flexible and applicable to a wide range of tasks, including forecasting, retrospective inference, and time series decomposition. Beyond microbiome studies, many other fields collect count-compositional time series. These include molecular biology Espinoza et al. (2020), natural language processing Linderman et al. (2015), biomedicine Fokianos and Kedem (2003), and social sciences Cargnoni et al. (1997). Our methods may be useful in those fields as well.

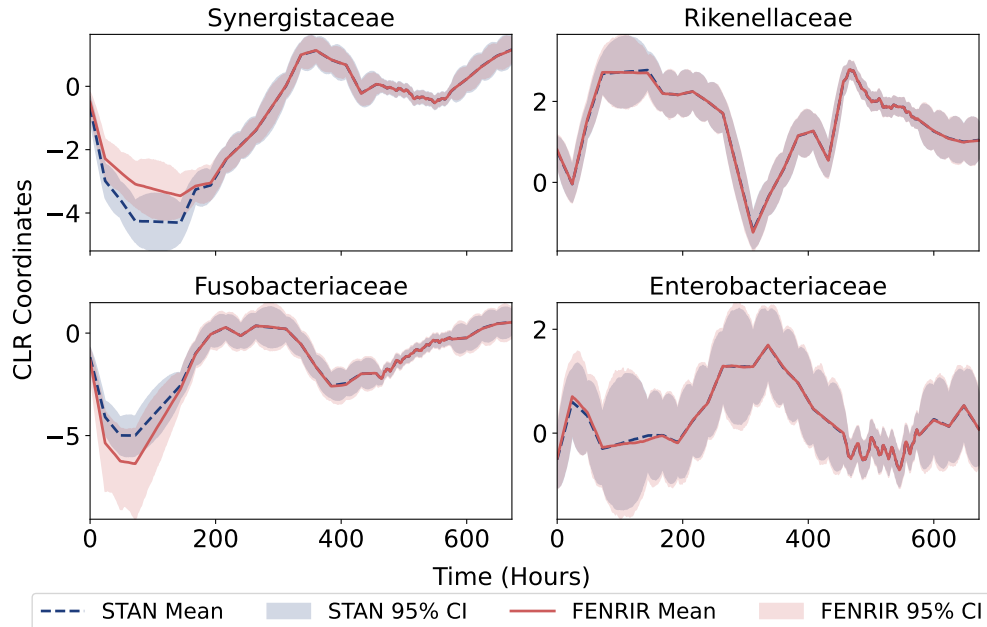


Figure 3: **Posterior mean and credible intervals for state Θ of MLN-DLM applied to Artificial Gut Microbiome Data.** For brevity, we show the posterior for Θ for four Centered Log-Ratio (CLR) coordinates (four dimensions) in Vessel 2. We highlight the two dimensions with the worst agreement between Fenrir and Stan (Synergistaceae and Fusobacteriaceae) to illustrate worse-case performance.

We have developed algorithms for approximate posterior inference. Our experiments show that the approximated posterior can be nearly identical to the true posterior. We suspect the approximation may be good enough to form the basis for an efficient, exact inference algorithm. Methods like importance resampling can refine posterior samples from an approximate model into samples from the exact posterior (Prado et al., 2021, Chapter 6). In particular, we suspect sequential particle methods, such as Sequential Importance Resampling or Particle MCMC, will prove particularly useful as they can exploit the structure of time series data.

This work focuses on state estimation using the Fenrir method described in the main text. While we have demonstrated joint estimation of state parameters and model hyperparameters using a Gibbs sampler, Gibbs schemes are not optimal for this task. In particular, slice sampling can lead to dramatic improvements when inferring covariance hyperparameters in latent Gaussian models (Murray and Adams, 2010). Still, Gibbs schemes are more straightforward and flexible. Remarkably, Fenrir was so efficient as to make even a simple Gibbs sampler almost 2.5 times more efficient than Stan. Overall, Gibbs samplers are likely a good starting point for researchers looking to include Fenrir in more complex models, but ultimately, more specialized methods (e.g., (Murray and Adams, 2010)) will prove substantially more efficient.

Our results on real data suggest a limitation of our approach that we suspect may not be addressed effectively by the aforementioned future directions. Based on Figure 3, we suspect that the accuracy of our Debiased Multinomial Dirichlet Bootstrap will deteriorate when analyzing time series that are highly sparse (few non-zero counts). This hypothesis is also informed by theoretical results relating to the CU sampler with marginal Laplace approximation (Silverman et al., 2022), suggesting a similar limitation. While our experimental results suggest our method works well even in the presence of moderate sparsity (e.g., microbiome data), we expect it will perform poorly at levels of sparsity encountered in categorical time series (e.g., natural language processing). As a result, we primarily recommend our method when analyzing multinomial (as opposed to categorical) time series.

References

- Äijö, T., Müller, C. L., and Bonneau, R. (2018). Temporal probabilistic modeling of bacterial compositions derived from 16s rRNA sequencing. *Bioinformatics*, 34(3):372–380.
- Aitchison, J. (1982). The statistical analysis of compositional data. *Journal of the Royal Statistical Society: Series B (Methodological)*, 44(2):139–160.
- Aitchison, J. and Shen, S. M. (1980). Logistic-normal distributions: Some properties and uses. *Biometrika*, 67(2):261–272.
- Cargnoni, C., Müller, P., and West, M. (1997). Bayesian forecasting of multinomial time series through conditionally gaussian dynamic models. *Journal of the American Statistical Association*, 92(438):640–647.
- Carpenter, B., Gelman, A., Hoffman, M. D., Lee, D., Goodrich, B., Betancourt, M., Brubaker, M. A., Guo, J., Li, P., and Riddell, A. (2017). Stan: A probabilistic programming language. *Journal of statistical software*, 76.
- Espinoza, J. L., Shah, N., Singh, S., Nelson, K. E., and Dupont, C. L. (2020). Applications of weighted association networks applied to compositional data in biology. *Environmental Microbiology*, 22(8):3020–3038.
- Fernandes, A. D., Reid, J. N., Macklaim, J. M., McMurrugh, T. A., Edgell, D. R., and Gloor, G. B. (2014). Unifying the analysis of high-throughput sequencing datasets: characterizing RNA-seq, 16S rRNA gene sequencing and selective growth experiments by compositional data analysis. *Microbiome*, 2(1):1–13.
- Fokianos, K. and Kedem, B. (2003). Regression theory for categorical time series. *Statistical Science*, 18(3):357–376.
- Friedman, J. and Alm, E. J. (2012). Inferring correlation networks from genomic survey data. *PLoS Computational Biology*, 8(9):e1002687.
- Glynn, C., Tokdar, S. T., Howard, B., and Banks, D. L. (2019). Bayesian Analysis of Dynamic Linear Topic Models. *Bayesian Analysis*, 14(1).
- Grantham, N. S., Guan, Y., Reich, B. J., Borer, E. T., and Gross, K. (2020). Mimix: A bayesian mixed-effects model for microbiome data from designed experiments. *Journal of the American Statistical Association*, 115(530):599–609.
- Joseph, T. A., Pasarkar, A. P., and Pe’er, I. (2020). Efficient and accurate inference of mixed microbial population trajectories from longitudinal count data. *Cell Systems*, 10(6):463–469.
- Linderman, S., Johnson, M. J., and Adams, R. P. (2015). Dependent multinomial models made easy: Stick-breaking with the pólya-gamma augmentation. *Advances in neural information processing systems*, 28.
- Mosimann, J. E. (1962). On the compound multinomial distribution, the multivariate β -distribution, and correlations among proportions. *Biometrika*, 49(1/2):65–82.
- Murray, I. and Adams, R. P. (2010). Slice sampling covariance hyperparameters of latent Gaussian models. *Advances in neural information processing systems*, 23.
- Nixon, M. P., Gloor, G. B., and Silverman, J. D. (2024). Beyond Normalization: Incorporating Scale Uncertainty in Microbiome and Gene Expression Analysis. *bioRxiv*.
- Nixon, M. P., Letourneau, J., David, L. A., Lazar, N. A., Mukherjee, S., and Silverman, J. D. (2023). Scale Reliant Inference. *arXiv*.
- Pawlowsky-Glahn, V., Egozcue, J. J., and Tolosana-Delgado, R. (2015). *Modeling and analysis of compositional data*. John Wiley & Sons.
- Polson, N. G., Scott, J. G., and Windle, J. (2013). Bayesian inference for logistic models using pólya-gamma latent variables. *Journal of the American statistical Association*, 108(504):1339–1349.
- Prado, R., Ferreira, M. A. R., and West, M. (2021). *Time Series: Modeling, Computation, and Inference*. Chapman and Hall/CRC, New York, 2 edition.
- Qiu, Y., Balan, S., Beall, M., Sauder, M., Okazaki, N., and Hahn, T. (2023). *RcppNumerical: ‘Rcpp’ Integration for Numerical Computing Libraries*. R package version 0.6-0.
- Silverman, J. D., Durand, H. K., Bloom, R. J., Mukherjee, S., and David, L. A. (2018). Dynamic linear models guide design and analysis of microbiota studies within artificial human guts. *Microbiome*, 6:1–20.
- Silverman, J. D., Roche, K., Holmes, Z. C., David, L. A., and Mukherjee, S. (2022). Bayesian multinomial logistic normal models through marginally latent matrix-t processes. *Journal of Machine Learning Research*, 23(7):1–42.
- West, M. and Harrison, J. (2006). *Bayesian forecasting and dynamic models*. Springer Science & Business Media.

6 ISSUES WITH MARGINALLY LTP FORM FOR MLN-DLM

Silverman et al. (2022) propose marginalizing MLN-DLM's to their Latent Matrix T-process form. In brief, they use a recursive filter to marginalize over the state space Θ and covariance Σ . The problem is that researchers often specify MLN-DLMs with non-stationary state-space models (e.g., random walks or other polynomial trends). We find this leads to numerical instability. While we do not attempt to review their entire proposed approach, we note that it requires calculation of the following matrix A with elements:

$$A_{t,t-k} = \begin{cases} \gamma_t + F_t^T \left[W_t + \sum_{l=t}^2 G_{t:l} W_{l-1} G_{l:t}^T + G_{t:1} C_0 G_{1:t}^T \right] F_t & \text{if } k = 0 \\ F_t^T \left[G_{t:t-k+1} W_{t-k} + \sum_{l=t-k}^2 G_{t:l} W_{l-1} G_{l:l-k}^T + G_{t:1} C_0 G_{1:t-k}^T \right] F_{t-k} & \text{if } k > 0 \end{cases} \quad (1)$$

where $G_{t:l}$ denotes short hand notation for the product $G_t \cdots G_l$.

Consider a simple univariate random walk model where $G = 1$. Even in this simple case, for long time series, the term $\sum_{l=t}^2 G_{t:l} W_{l-1} G_{l:t}^T$ explodes as there is linear accumulation of the state variances W_{l-1} . The problem gets worse with more complicated models (e.g., first or second order polynomial models) where the summation leads to quadratic or cubic accumulation. In practice, numerical errors start to dominate the computation and the resultant matrix A .

The key problem of the Silverman et al. (2022) method is the need to pre-compute the prior over the entire time series – which requires the matrix A . Instead, our approach avoids this issue. Like the Kalman filter, we only compute the prior one-step ahead of each observation. This stabilizes both our calculation of prior densities (e.g., $p(\eta)$) and gradients of those densities.

7 FILTERING AND SMOOTHING EQUATIONS

The following equations define a recursive filter and smoother for the multivariate DLM described in Section 3 of main text. These equations are reproduced from Silverman et al. (2022) who reproduced them from Prado et al. (2021).

Filtering recursion:

(1) Posterior at $t - 1$:

$$\begin{aligned} p(\Sigma|H_{t-1}^T) &\sim IW(\Xi_{t-1}, \nu_{t-1}) \\ p(\Theta_{t-1}|\Sigma, H_{t-1}^T) &\sim \mathcal{N}(M_{t-1}, C_{t-1}, \Sigma) \end{aligned}$$

(2) Prior at t :

$$\begin{aligned} A_t &= G_t M_{t-1} \\ R_t &= G_t C_{t-1} G_t^T + W_t \\ p(\Sigma|H_{t-1}^T) &\sim IW(\Xi_{t-1}, \nu_{t-1}) \\ p(\Theta_t|\Sigma, H_{t-1}^T) &\sim \mathcal{N}(A_t, R_t, \Sigma) \end{aligned}$$

(3) One-step ahead forecast at t :

$$\begin{aligned} f_t^T &= F_t^T A_t \\ q_t &= \gamma_t + F_t^T R_t F_t \\ p(\Sigma|H_{t-1}^T) &\sim IW(\Xi_{t-1}, \nu_{t-1}) \\ p(\eta_t|\Sigma, H_{t-1}^T) &\sim \mathcal{N}(f_t, q_t \Sigma) \end{aligned}$$

(4) Posterior at t :

$$\begin{aligned} e_t^T &= \eta_t^T - f_t^T \\ S_t &= \frac{R_t F_t}{q_t} \\ M_t &= A_t + S_t e_t^T \\ C_t &= R_t - q_t S_t S_t^T \\ \nu_t &= \nu_{t-1} + 1 \\ \Xi_t &= \Xi_{t-1} + \frac{e_t e_t^T}{q_t} \\ p(\Sigma|H_{t-1}^T) &\sim IW(\Xi_t, \nu_t) \\ p(\Theta_t|\Sigma, H_{t-1}^T) &\sim \mathcal{N}(M_t, C_t, \Sigma) \end{aligned}$$

Smoothing Recursion:

1. Sample $\Sigma \sim IW(\Xi_T, \nu_T)$ and then $\Theta_T \sim \mathcal{N}(M_T, C_T, \Sigma)$.
2. For each time t from $T - 1$ to 0, sample $p(\Theta_t|\Theta_{t+1}, H_T^T)$ from $\mathcal{N}(M_t^*, C_t^*, \Sigma)$ where

$$\begin{aligned} Z_t &= C_t G_{t+1}^T R_{t+1}^{-1} \\ M_t^* &= M_t + Z_t (\Theta_{t+1} - A_{t+1}) \\ C_t^* &= C_t - Z_t R_{t+1} Z_t^T \end{aligned}$$

where $H_{t-1} = (\eta_{t-1}, \dots, \eta_1)$.

8 CALCULATION OF GRADIENTS FOR MAP ESTIMATION OF η

As mentioned in the main text Section 3.2, we obtain MAP estimates of η within the collapsed model:

$$\hat{\eta} = \underset{\eta \in \mathbb{R}^{(D-1) \times T}}{\operatorname{argmin}} [-\log p(\eta | Y)].$$

By Bayes rule, the collapsed model can be partitioned into two parts:

$$-\log p(\eta | Y) \propto \underbrace{-\sum_t \log \operatorname{Multinomial}(Y_{\cdot t} | \phi^{-1}(\eta_{\cdot t}))}_I \underbrace{-\log p(\eta)}_{II} \quad (2)$$

The gradients for term I (denoted as g below) were already provided by Silverman et al. (2022) and are given as follows:

$$\begin{aligned} g &= \sum_{j=1}^T \left(\sum_{i=1}^{D-1} \eta_{ij} Y_{ij} - n_j \log \left(1 + \sum_{i=1}^{D-1} e^{\eta_{ij}} \right) \right) \\ O &= \exp \eta \\ m &= \mathbf{1}_N + O^T \mathbf{1}_{D-1} \\ \rho &= \operatorname{vec}(O) \odot \operatorname{vec}(\mathbf{1}_{D-1} m^T) \\ n &= \mathbf{1}_D^T Y \\ g &= \operatorname{vec}(\eta)^T \operatorname{vec}(Y_{/D}) - n \odot \log(m) \\ \frac{dg}{d\operatorname{vec}(\eta)} &= (\operatorname{vec}(Y_{/D}) - \operatorname{vec}(\mathbf{1}_{D-1} n) \odot \rho)^T \end{aligned}$$

where $\exp X$ and $\log X$ refers to the element-wise exponentiation and logarithm of a matrix X , \odot and \oslash refer to element-wise product and division respectively, and $Y_{/D}$ represents the first $D - 1$ rows of the matrix Y .

Term II in equation 2, as described in the main text's Section 3.2 follows a multivariate t-distribution with log probability:

$$\log p(\eta_t | H_{t-1}^T) \propto \frac{-(\nu_{t-1} + p)}{2} \log \left(1 + \frac{1}{\nu_{t-1}} (\eta_t - f_t)^T (q_t \Xi_{t-1})^{-1} (\eta_t - f_t) \right)$$

For getting the gradient, we would like to calculate $\frac{d \log |L|}{d\eta_t}$, where $L = 1 + \frac{1}{\nu_{t-1}} (\eta_t - f_t)^T (q_t \Xi_{t-1})^{-1} (\eta_t - f_t)$:

$$\frac{d \log |L|}{d\eta_t} = \frac{1}{L} \frac{dL}{d\eta_t}$$

$$\begin{aligned} dL &= d \left(\frac{1}{\nu_{t-1}} [(\eta_t - f_t)^T X^{-1} (\eta_t - f_t)] \right) \\ &= \frac{1}{\nu_{t-1}} [d\eta_t^T (X^{-1} \eta_t - X^{-1} f_t) + (\eta_t^T X^{-1} - f_t^T X^{-1}) d\eta_t] \\ &= \frac{1}{\nu_{t-1}} [(\eta_t^T X^{-1} - f_t^T X^{-1}) d\eta_t + (\eta_t^T X^{-1} - f_t^T X^{-1}) d\eta_t] \\ \frac{dL}{d\eta_t} &= \frac{2}{\nu_{t-1}} (\eta_t^T - f_t^T) X^{-1} \end{aligned}$$

where $X = (q_t \Xi_{t-1})$

9 MISSING OBSERVATIONS

Missing observations are easy to handle as modifications of the filtering recursion in Section 7. If the t -th time-point is missing, we simply skip the posterior update and let the prior equal the posterior:

$$\begin{aligned}
 M_t &= A_t \\
 C_t &= R_t \\
 \nu_t &= \nu_{t-1} \\
 \Xi_t &= \Xi_{t-1} \\
 p(\Sigma \mid H_{t-1}^T) &\sim \text{IW}(\Xi_t, \nu_t) \\
 p(\Theta_t \mid \Sigma, H_t^T) &\sim \mathcal{N}(M_t, C_t, \Sigma)
 \end{aligned}$$

10 MULTIPLE TIME SERIES

The following figure is a graphic depiction of how we handle multiple time-series. In this figure superscripts denote the index of one of K time-series. Only the filtration over Ξ and ν occur as if all K time-series were a single long series. For all other parameters filtering and smoothing occur as if the time-series were independent. For example, the state filtration resets to the prior (M_0, C_0) when the filter encounters the start of a new series. Similarly smoothing occurs as if the series were independent. Note that our procedure is invariant to the ordering of the K series.

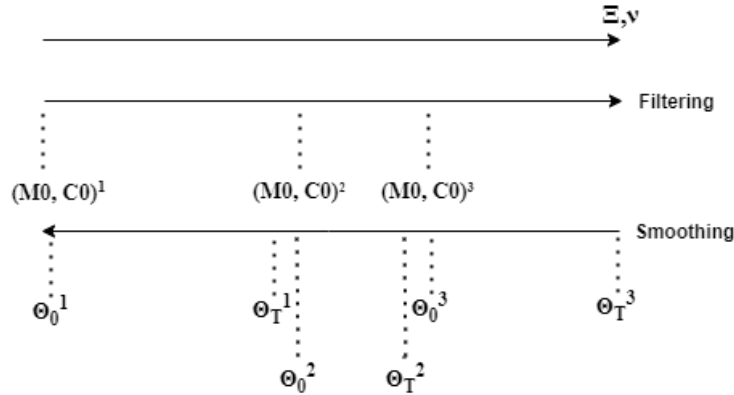


Figure 4: Multiple Time Series

The following algorithms defines our approach more formally.

Algorithm 1: Filtering for Multiple Time Series**Input:** $\eta, F, G, \gamma, W, M_0, C_0, \Xi_0, \nu_0, N, K$

```

1  $t = 0$ 
2  $A, R, f, q, S, e, M, C, \Xi, \nu \leftarrow \emptyset$ 
3 for  $k = 0 \rightarrow K$  do
4    $M_{t+k} \leftarrow M_0(k)$ 
5    $C_{t+k} \leftarrow C_0(k)$ 
6   for  $i = 0 \rightarrow N(k)$  do
7     // Prior
8      $A_t \leftarrow G_t M_{t+k}$ 
9      $R_t \leftarrow G_t C_{t+k} G_t^T + W_t$ 
10    // One-step ahead forecast
11     $f_t \leftarrow A_t^T F_t$ 
12     $q_t \leftarrow F_t^T R_t F_t + \gamma_t$ 
13    // Posterior
14     $S_t \leftarrow R_t F_t / q_t$ 
15     $e_t \leftarrow \eta_t - f_t$ 
16     $M_{t+k+1} \leftarrow A_t + S_t e^T$ 
17     $C_{t+k+1} \leftarrow R_t - q_t S_t S_t^T$ 
18     $\nu_{t+1} \leftarrow \nu_t + 1$ 
19     $\Xi_{t+1} \leftarrow \Xi_t + (e_t e_t^T) / q_t$ 
20     $t \leftarrow t + 1$ 
21 return  $A, R, f, q, S, e, M, C, \Xi, \nu$ 

```

Algorithm 2: Smoothing for Muple Time Series

Input: $\Xi, \nu, K, N, C, M, G, R, A, seed$

```

1   $rng \leftarrow \text{random}(seed)$ 
2   $\Xi_T \leftarrow (\Xi_T + \Xi_T^T)/2$ 
3   $\Sigma \leftarrow \text{inv\_wishart\_rng}(\nu_T, \Xi_T, rng)$ 
4   $\Sigma \leftarrow (\Sigma + \Sigma^T)/2.0$ 
5   $t \leftarrow -1$ 
6   $reset\_flag \leftarrow 1$ 
7   $Z, \Theta, \Theta_0 \leftarrow \emptyset$ 
8  for  $k = K - 1 \rightarrow 0$  do
9       $reset\_flag \leftarrow 1$ 
10     for  $i = 0 \rightarrow N(k)$  do
11         if  $reset\_flag == 1$  then
12              $C_{T+k-t-1} \leftarrow (C_{T+k-t-1} + C_{T+k-t-1}^T)/2.0$ 
13              $\theta_{T-t-2} \leftarrow \text{matrix\_normal\_rng}(M_{T+k-t-1}, C_{T+k-t-1}, \Sigma, rng)$ 
14              $reset\_flag \leftarrow 0$ 
15         else
16              $G_t \leftarrow G_{T-t-1}$ 
17              $Z \leftarrow C_{T+k-t-1} G_t^T R_{T-t-1}^{-1}$ 
18              $C_{T+k-t-1} \leftarrow C_{T+k-t-1} - Z R_{T-t-1} Z^T$ 
19              $C_{T+k-t-1} \leftarrow (C_{T+k-t-1} + C_{T+k-t-1}^T)/2.0$ 
20              $M_{T+k-t-1} \leftarrow M_{T+k-t-1} + Z(\theta_{T-t-1} - A_{T-t-1})$ 
21              $\theta_{T-t-2} \leftarrow \text{matrix\_normal\_rng}(M_{T+k-t-1}, C_{T+k-t-1}, \Sigma, rng)$ 
22             if  $i == N(k) - 1$  then
23                  $G_t \leftarrow G_{T-t-2}$ 
24                  $Z \leftarrow C_{T+k-t-2} G_t^T R_{T-t-2}^{-1}$ 
25                  $C_{T+k-t-2} \leftarrow C_{T+k-t-2} - Z R_{T-t-2} Z^T$ 
26                  $C_{T+k-t-2} \leftarrow (C_{T+k-t-2} + C_{T+k-t-2}^T)/2.0$ 
27                  $M_{T+k-t-2} \leftarrow M_{T+k-t-2} + Z(\theta_{T-t-2} - A_{T-t-2})$ 
28                  $\theta_0(k) \leftarrow \text{matrix\_normal\_rng}(M_{T+k-t-2}, C_{T+k-t-2}, \Sigma, rng)$ 
29 return  $\Theta, \Theta_0, \Sigma$ 

```

11 HYPERPARAMETER INFERENCE

In Section 3.7 of the main text, we extend our MLN-DLM model by placing a prior on the hyperparameter $W = \text{diag}(w_1, \dots, w_Q)$ to make it learnable and introduce a simple Gibbs sampling approach for inference. This is achieved by sampling from the posterior $p(\Theta, \Sigma, \eta, w_1, \dots, w_Q \mid Y)$ using Gibbs updates. Below, we expand on this and provide a detailed explanation of the process.

In main text, we outline our approach to sampling the conditional posterior $p(\Theta, \Sigma, \eta \mid Y, W)$. We now develop the complementary Gibbs steps for $p(w_1, \dots, w_Q \mid Y, \Theta, \eta, \Sigma)$. Note that, by conditional independence, this reduces to $p(w_1, \dots, w_Q \mid \Theta, \Sigma)$.

In terms of the conditional $p(w_1, \dots, w_Q \mid \Theta, \Sigma)$, the relevant parts of the MLN-DLM model are

$$\begin{aligned} \Theta_t &= G_t \Theta_{t-1} + \Omega_t, \quad \Omega_t \sim \mathcal{N}(0, W, \Sigma) \\ W &= \begin{bmatrix} w_1 & \cdots & 0 \\ \vdots & \ddots & \vdots \\ 0 & \cdots & w_Q \end{bmatrix} \\ w_q &\sim \text{InvGamma}(a_q, b_q) \end{aligned}$$

Letting $L = \text{Cholesky}(\Sigma^{-1})$, and letting $\Omega_t^* = \Omega_t L$ this model can be reparameterized as

$$\begin{aligned} \Omega_{ti}^* &\sim \mathcal{N}(0, W) \\ W &= \begin{bmatrix} w_1 & \cdots & 0 \\ \vdots & \ddots & \vdots \\ 0 & \cdots & w_Q \end{bmatrix} \\ w_q &\sim \text{InvGamma}(a_q, b_q) \end{aligned}$$

A blocked Gibbs step can be used to update each w_1, \dots, w_Q . Each is updated as a standard, conjugate normal-inverse gamma model with posterior $p(w_q \mid \Omega_q^*) = \text{InvGamma}(a_q^*, b_q^*)$. The parameters of the posterior are given by

$$\begin{aligned} a_q^* &= a_q + T(D - 1) \\ b_q^* &= \frac{1}{a_q^*} \left(a_q b_q^2 + \sum_{t,i} [\Omega_{qti}^* - \overline{\Omega}_q^*]^2 \right) \end{aligned}$$

where $\overline{\Omega}_q^*$ denotes the sample mean of the $T \times (D - 1)$ elements in the matrix $\Omega_q^* = [\Omega_{q1}^*, \dots, \Omega_{qT}^*]$.

12 SIMULATIONS

In this section, we give the full details of the data simulation procedure briefly mentioned in the main text’s Section 4.1. Also, we provide the results of uncertainty quantification when number of multinomial categories $D = 10$ with $T = 300$ to show that our conclusions on the smaller simulation hold in higher dimensions.

12.1 Data Simulation Model

We use the MLN-DLM model with the following specified priors to generate simulated data:

$$\begin{aligned}
 Y_{.t} &\sim \text{Multinomial}(\pi_{.t}) \\
 \pi_{.t} &= \phi^{-1}(\eta_{.t}) \\
 \eta_{.t}^T &= \Theta_t + v_t^T \quad v_t \sim \mathcal{N}(0, \Sigma) \\
 \Theta_t &= \Theta_{t-1} + \Omega_t, \quad \Omega_t \sim \mathcal{N}(0, 0.45, \Sigma) \\
 \Theta_0 &\sim \mathcal{N}(M_0, C_0, \Sigma) \\
 \Sigma &\sim IW(I, D + 3) \\
 M_0 &\sim \text{Uniform}(0.1, 1) \\
 C_0 &\sim \text{Uniform}(1, 1.5)
 \end{aligned}$$

Each simulation consists of multiple time series, with 5% of the time points randomly missing in each series. While each time series has its own state parameters Θ_t , information about other parameters (e.g., Σ) is shared across the series. Every time series contains 100 time points, and the total number of time series depends on the overall number of time points. For example, 1,000 total time points would correspond to 10 time series, each with 100 time points.

12.2 Considerations during Uncertainty Quantification

While generating Debiased Multinomial Dirichlet Samples for Uncertainty Quantification in Fenrir, we choose the pseudocount parameter $\alpha = 0.5$ and generate 2000 samples. For Stan, we run 4 chains, each with 4500 iterations, taking the first 1500 as warmup.

12.3 Results of Uncertainty Quantification for Simulated Data when $D = 10$

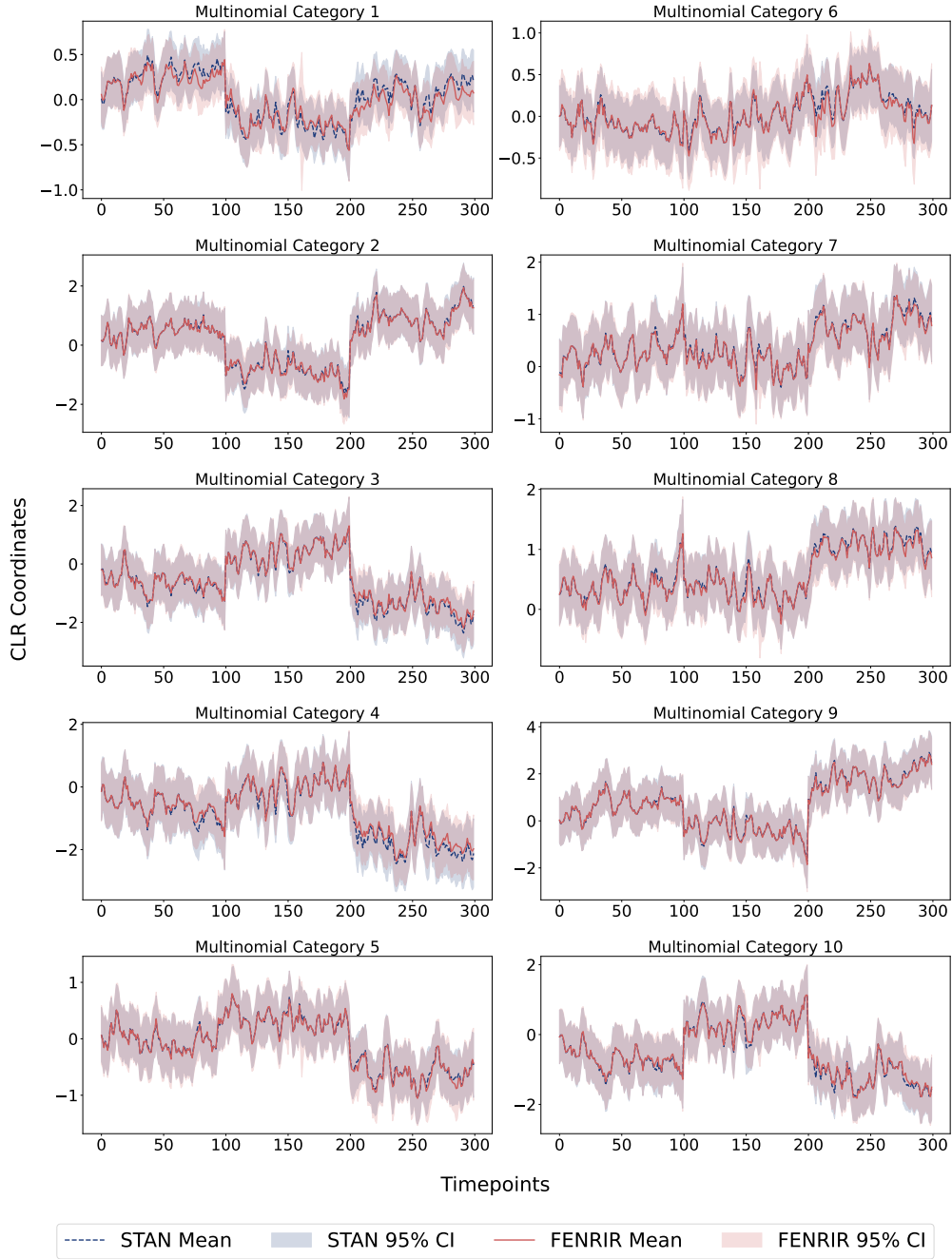


Figure 5: **Posterior mean and credible intervals for Θ of MLN-DLM applied to simulated data.** We compare Fenrir and our Stan implementation results on simulated data with $D = 10$ and $T = 300$, showing posterior means and 95% credible intervals. The posterior is depicted using centered log-ratio (CLR) coordinates, with each coordinate corresponding to a different multinomial category.

13 ARTIFICIAL GUT MICROBIOME DATA

We obtained data from the artificial gut study, presented in the main text’s Section 4.2, from the R package Fido (github.com/jsilve24/fido). The data is available in that package as the data object *mallard_family*. This data contains observations recorded at irregular intervals; the study consisted of both daily hourly sampling. Our analyses occur at hourly time-scales. As a result, we padded the original data with missing values so the entire series can be represented as hourly.

In the following subsections, we provide details of the MLN-DLM model with prior specifications used to produce the results discussed in Section 4.2 of the main text. We also present the posterior estimates of the hyperparameter $W = \text{diag}(w_1)$, as well as the posterior inference results for state Θ across all taxa and vessels.

13.1 MLN-DLM Model Specification

Both Fenrir and Stan fit the model specified below to produce the results here and in the main text.

$$\begin{aligned}
 Y_{.t} &\sim \text{Multinomial}(\pi_{.t}) \\
 \pi_{.t} &= \phi^{-1}(\eta_{.t}) \\
 \eta_t^T &= \Theta_t + v_t^T \quad v \sim \mathcal{N}(0, \Sigma) \\
 \Theta_t &= \Theta_{t-1} + \Omega_t, \quad \Omega_t \sim \mathcal{N}(0, w_1, \Sigma) \\
 \Theta_0 &\sim \mathcal{N}(0, 1, \Sigma) \\
 \Sigma &\sim IW(10I, D + 3) \\
 w_1 &\sim \text{InverseGamma}(30, 15)
 \end{aligned}$$

13.2 Maximum A Posteriori (MAP) estimation Results

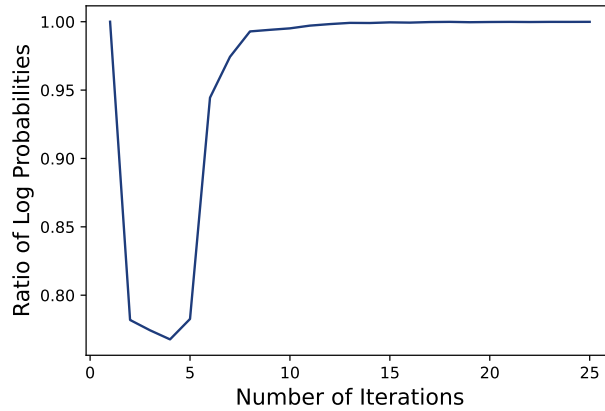


Figure 6: **Ratio of log probabilities of Fenrir and our Stan implementation for MAP estimation of η applied to Artificial Gut Microbiome Data**

13.3 Additional Posterior Inference Results

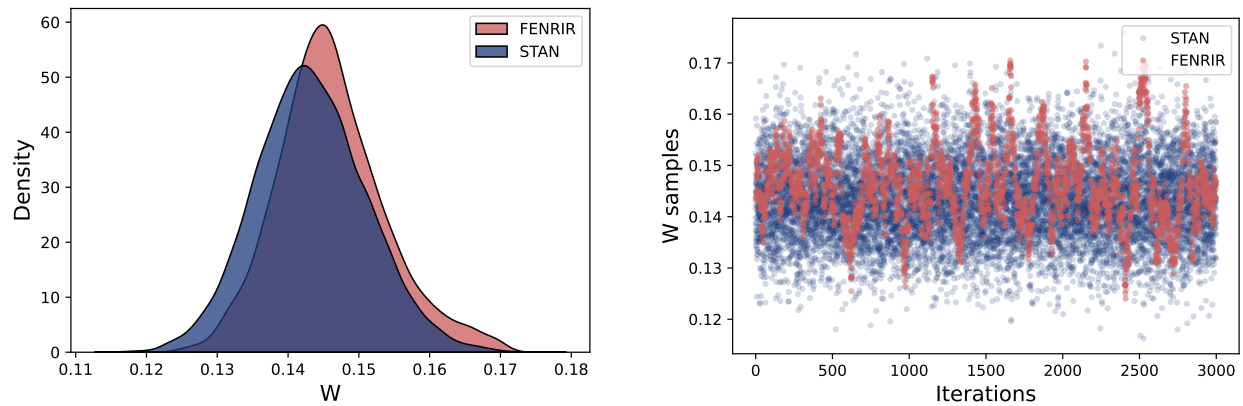


Figure 7: **Posterior Estimates for hyperparameter W from Fenrir-based Gibbs sampler and Stan.** The left plot shows the density of posterior samples for W and the right plot illustrates the trace of W samples across 3000 iterations.

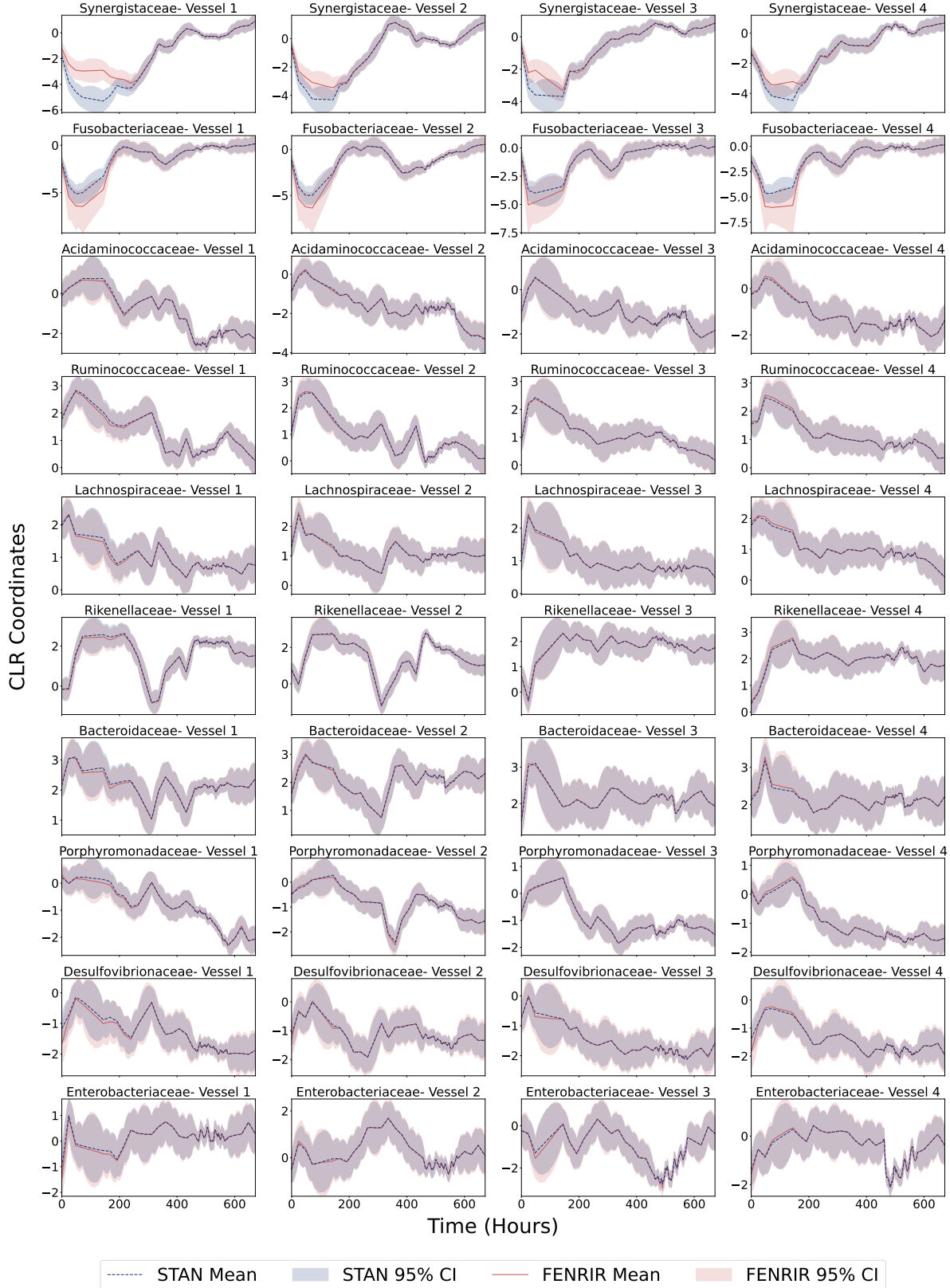


Figure 8: **Posterior mean and credible intervals for state Θ of MLN-DLM applied to Artificial Gut Microbiome Data.** We compare Fenrir and our Stan implementation results of all 10 taxa and all 4 vessels, showing posterior means and 95% credible intervals. The posterior is depicted using centered log-ratio (CLR) coordinates, with each coordinate corresponding to a different multinomial category.

14 LOCAL TREND MLN-DLM MODEL

In this section, we aim to demonstrate that Fenrir can model more complex state-space dynamics, such as incorporating a local trend or velocity term. We achieve this by adjusting the MLN-DLM model described in Section 3 of the main text.

$$\begin{aligned}
 Y_{.t} &\sim \text{Multinomial}(\pi_{.t}) \\
 \pi_{.t} &= \phi^{-1}(\eta_{.t}) \\
 \eta_t^T &= F_t^T \begin{bmatrix} \Theta_t \\ \alpha_t \end{bmatrix} + v_t^T \quad v_t \sim \mathcal{N}(0, \gamma_t \Sigma) \\
 \begin{bmatrix} \Theta_t \\ \alpha_t \end{bmatrix} &= G_t \begin{bmatrix} \Theta_{t-1} \\ \alpha_{t-1} \end{bmatrix} + \begin{bmatrix} \Omega_{\Theta t} \\ \Omega_{\alpha t} \end{bmatrix}, \quad \begin{bmatrix} \Omega_{\Theta t} \\ \Omega_{\alpha t} \end{bmatrix} \sim \mathcal{N}\left(0, \begin{bmatrix} w_{\Theta} & 0 \\ 0 & w_{\alpha} \end{bmatrix}, \Sigma\right) \\
 \begin{bmatrix} \Theta_0 \\ \alpha_0 \end{bmatrix} &\sim \mathcal{N}(M_0, C_0, \Sigma) \\
 \Sigma &\sim IW(\Xi, \nu)
 \end{aligned}$$

We can extend the above model by including a prior over w_{Θ} and w_{α} :

$$\begin{aligned}
 w_{\Theta} &\sim \text{InvGamma}(a, b) \\
 w_{\alpha} &\sim \text{InvGamma}(c, d)
 \end{aligned}$$

We follow similar steps as in Section 3.7 of the main text to derive the posterior conditionals and set up our naive Fenrir-based Gibbs sampler for the model above. Sampling from $p(\Theta, \Sigma, \eta \mid Y, W)$ remains the same as discussed in the main text, while $p(w_{\Theta}, w_{\alpha} \mid \Theta, \Sigma)$ is derived below.

Letting $L = \text{Cholesky}(\Sigma^{-1})$, and letting $\begin{bmatrix} \Omega_{\Theta t} \\ \Omega_{\alpha t} \end{bmatrix}^* = \begin{bmatrix} \Omega_{\Theta t} \\ \Omega_{\alpha t} \end{bmatrix} L$, this model can be reparameterized as

$$\begin{aligned}
 \begin{bmatrix} \Omega_{\Theta ti} \\ \Omega_{\alpha ti} \end{bmatrix}^* &\sim N\left(0, \begin{bmatrix} w_{\Theta} & 0 \\ 0 & w_{\alpha} \end{bmatrix}\right) \\
 w_{\Theta} &\sim \text{InvGamma}(a, b) \\
 w_{\alpha} &\sim \text{InvGamma}(c, d)
 \end{aligned}$$

Since w_{Θ} and w_{α} are both independent, we can simply calculate the respective posteriors.

$$\begin{aligned}
 p(w_{\Theta} \mid \Omega_{\Theta}^*) &= \text{InvGamma}(a^*, b^*) \\
 p(w_{\alpha} \mid \Omega_{\alpha}^*) &= \text{InvGamma}(c^*, d^*) \\
 a^* &= a + T(D - 1) \\
 b^* &= \frac{1}{a^*} \left(ab^2 + \sum_{t,i} [\Omega_{\Theta ti}^* - \overline{\Omega_{\Theta}^*}]^2 \right) \\
 c^* &= c + T(D - 1) \\
 d^* &= \frac{1}{c^*} \left(cd^2 + \sum_{t,i} [\Omega_{\alpha ti}^* - \overline{\Omega_{\alpha}^*}]^2 \right)
 \end{aligned}$$

where $\overline{\Omega^*}$ denotes the sample mean of the $T \times (D - 1)$ elements in the matrix $\Omega^* = [\Omega_1^*, \dots, \Omega_T^*]$.

We specify the model defined above with the following prior specifications and fit it to the same artificial gut microbiome data discussed in Section 4.2 of the main text.

$$\begin{aligned}
 Y_{.t} &\sim \text{Multinomial}(\pi_{.t}) \\
 \pi_{.t} &= \phi^{-1}(\eta_{.t}) \\
 \eta_{.t}^T &= [1 \quad 0] \begin{bmatrix} \Theta_t \\ \alpha_t \end{bmatrix} + v_t^T \quad v_t \sim \mathcal{N}(0, \Sigma) \\
 \begin{bmatrix} \Theta_t \\ \alpha_t \end{bmatrix} &= \begin{bmatrix} 1 & 1 \\ 0 & 0.9 \end{bmatrix} \begin{bmatrix} \Theta_{t-1} \\ \alpha_{t-1} \end{bmatrix} + \Omega_t, \quad \Omega_t \sim \mathcal{N}\left(0, \begin{bmatrix} w_\Theta & 0 \\ 0 & w_\alpha \end{bmatrix}, \Sigma\right) \\
 \begin{bmatrix} \Theta_0 \\ \alpha_0 \end{bmatrix} &\sim \mathcal{N}(0, I, \Sigma) \\
 \Sigma &\sim IW(10I, D + 3) \\
 w_\Theta &\sim \text{InvGamma}(30, 15) \\
 w_\alpha &\sim \text{InvGamma}(30, 8)
 \end{aligned}$$

The figures below show the posterior inference of state Θ and state α across all taxa and all four vessels of the artificial gut microbiome data producing nearly identical posterior estimates for both methods. Regarding the posterior inference of hyperparameter W , our Gibbs sampler produced 3000 samples in 1.4 hours, while Stan took 12 hours to generate the same number. The posterior estimates of w_Θ and w_α were identical, with Fenrir estimating a posterior mean and 95% credible interval of 0.12 (0.104–0.135) for w_Θ and 0.02 (0.019–0.022) for w_α , and Stan estimating a posterior mean and 95% credible interval of 0.118 (0.104–0.135) for w_Θ and 0.02 (0.019–0.022) for w_α . Again even with a simple, naive Gibbs sampler, our approach produced approximately 0.58 effective samples per second for both state Θ and α , compared to Stan’s 0.26 and 0.27, respectively, for the two states. We conclude that our approach is approximately twice as fast as Stan with only minimal error in posterior estimates even when modeling complex state-space dynamics.

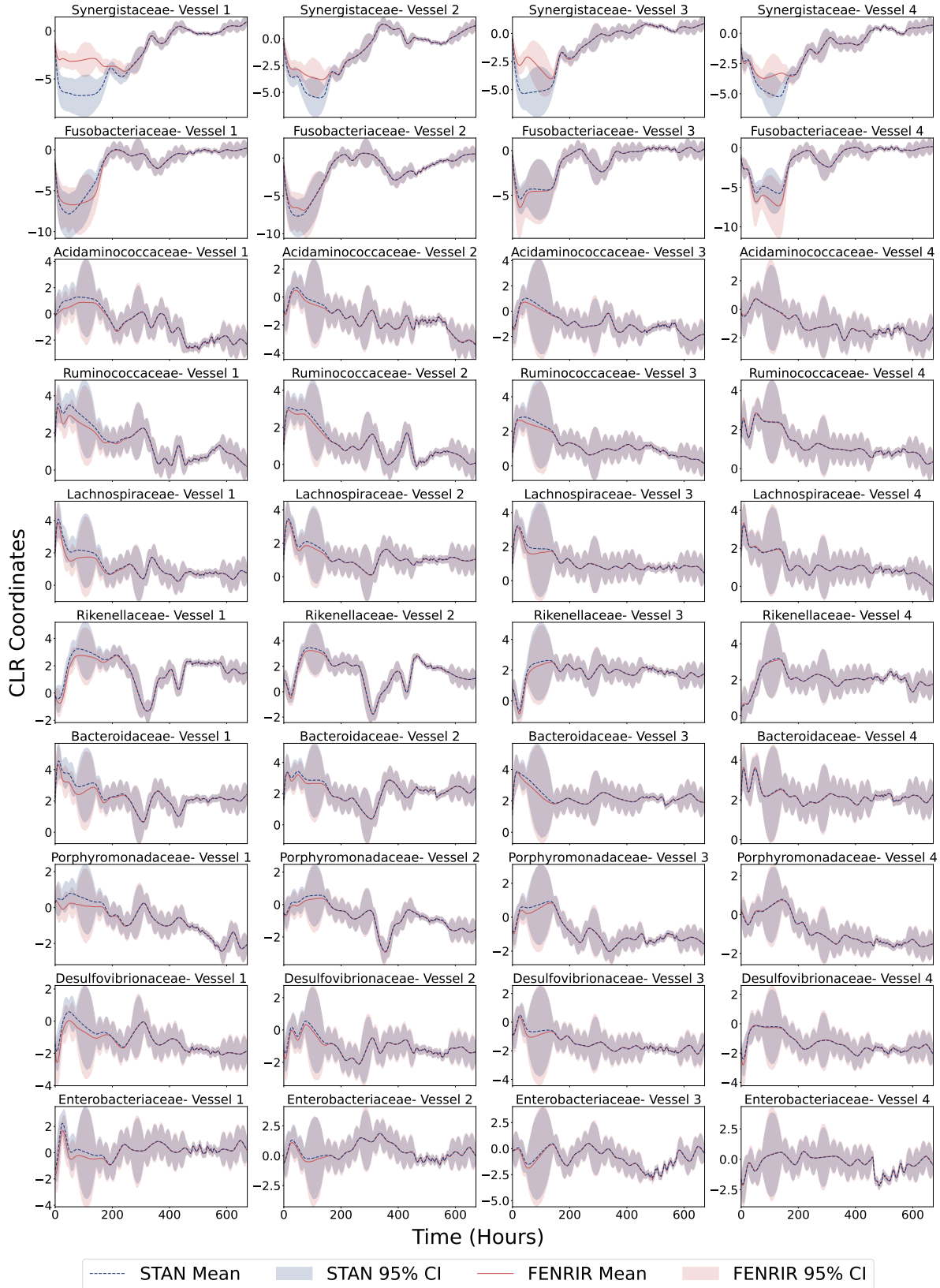


Figure 9: **Posterior mean and credible intervals for state Θ of local trend MLN-DLM model applied to Artificial Gut Microbiome Data.** We compare Fenrir and our Stan implementation results of all 10 taxa and all 4 vessels, showing posterior means and 95% credible intervals. The posterior is depicted using centered log-ratio (CLR) coordinates, with each coordinate corresponding to a different multinomial category.

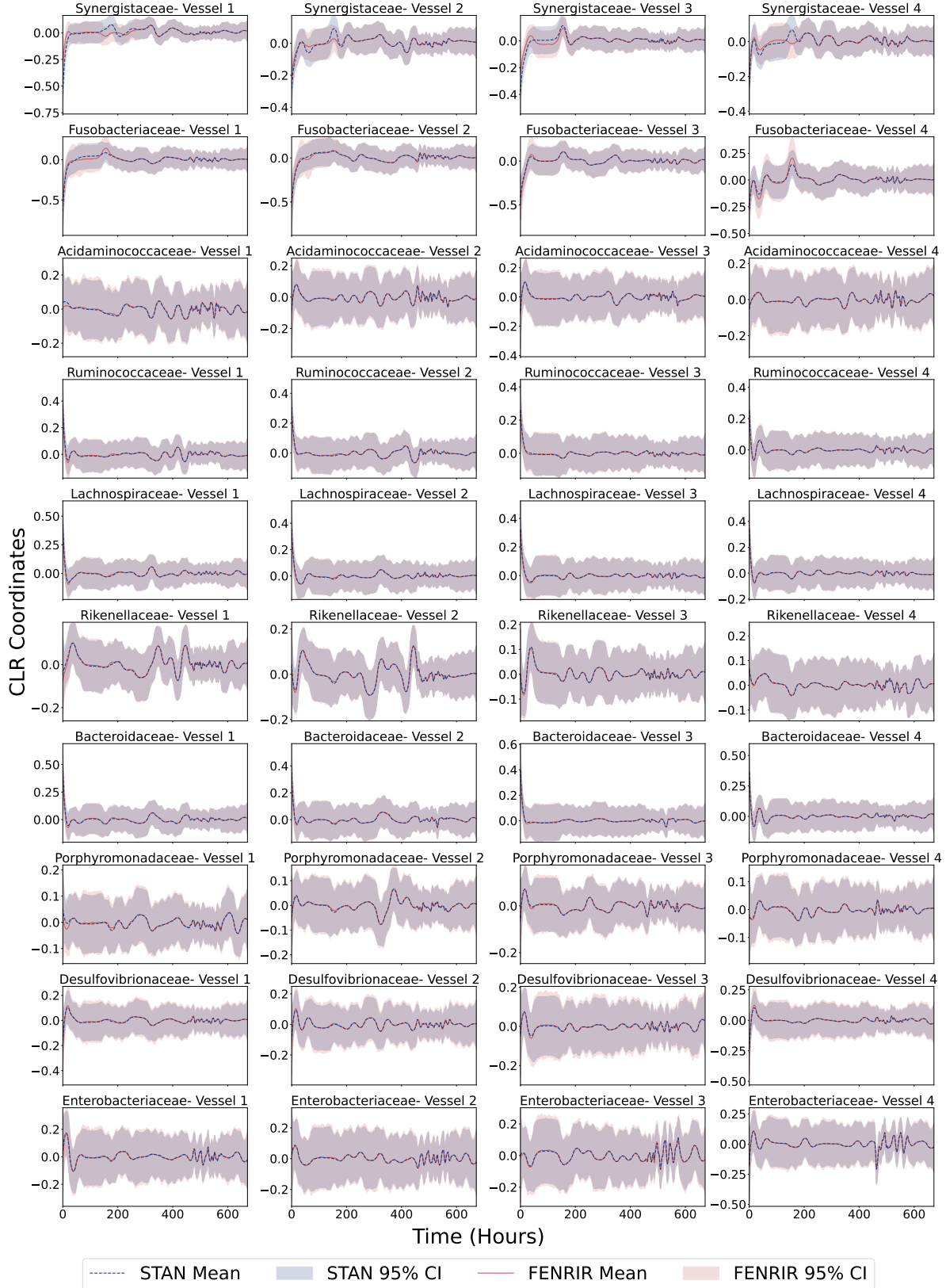


Figure 10: **Posterior mean and credible intervals for state α of local trend MLN-DLM model applied to Artificial Gut Microbiome Data.** We compare Fenrir and our Stan implementation results of all 10 taxa and all 4 vessels, showing posterior means and 95% credible intervals. The posterior is depicted using centered log-ratio (CLR) coordinates, with each coordinate corresponding to a different multinomial category.